

Full length article

# Ab initio study of beryllium surfaces with different hydrogen coverages

D.V. Bachurin<sup>\*</sup>, P.V. Vladimirov

Institute for Applied Materials Applied Materials Physics, Karlsruhe Institute of Technology, 76344, Eggenstein-Leopoldshafen, Germany

## ARTICLE INFO

### Keywords:

Ab initio calculations

Beryllium

Hydrogen

Surface energy

Interplanar relaxation

Equilibrium shape of a crystal

## ABSTRACT

The effect of hydrogen concentration on principal hexagonal close packed beryllium surfaces (basal, prismatic type I and II, pyramidal type I and II) at 0 K was studied with the help of *ab initio* methods. The configurations with critical hydrogen coverage were revealed. Relaxation of outermost atomic layers at critical coverage drastically differs from that found for clean beryllium surfaces. The presence of hydrogen atoms significantly changes the energy of all studied beryllium surfaces except for prismatic type II plane. Influence of hydrogen concentration on equilibrium shape of hydrogen covered voids was investigated by means of construction of Wulff polyhedra. In addition we generalized Gibbs Wulff approach for accounting of different hydrogen coverages at crystallographic non equivalent surfaces and temperature effect. The results of the construction were compared with classical Gibbs Wulff approach as well as the available experimental data on ion or neutron irradiation at elevated temperatures.

## 1. Introduction

Beryllium has a number of remarkable physical properties. Being very light and possessing high hardness, beryllium is commonly used as an alloy component for aerospace and aircraft industry to increase alloys' strength, fatigue and corrosion resistance, anti galling characteristics etc [1–3]. In nuclear industry beryllium is widely used as neutron reflector and moderator [4].

Light chemical elements (Be, Li, Mg and Al) are preferable for maximization of hydrogen storage per unit mass [5–8]. Therefore various beryllium compounds are studied as prospective hydrogen storage materials [9–13]. Consequently, theoretical study of various mechanisms of hydrogen trapping in metals is important for practical realization of hydrogen driven vehicles [14].

Besides impurities, hydrogen can be trapped by intrinsic defects in metals such as vacancies, dislocations, grain boundaries and pores [15]. Fukai and co workers have shown experimentally that for some metals loaded with hydrogen at high temperature and pressure anomalously high vacancy concentration of about 10 at.% was observed. They found that for metals with low vacancy formation energy this process usually results in formation of metal

hydrides with high hydrogen gravimetric density, which is important characteristic of candidate materials for hydrogen storage.

The second light metallic chemical element, beryllium, with its vacancy formation energy as low as 0.8 eV [16] could be by far one of the most encouraging metals for these applications. However, relatively high binding energy of hydrogen with vacancy ( $\sim 1.3$  eV) [16] suggests somewhat higher temperature ( $\sim 300$  °C) of its release than would be economically desirable for hydrogen storage ( $\sim 200$  °C, see Ref. [5]). Multiple hydrogen occupation of vacancy is possible and results in a gradual decrease of the binding energy with increase of the number of trapped hydrogen atoms [16]. Nevertheless, complete hydrogen release (de trapping of the last most bound hydrogen atoms within a vacancy) is possible only at higher temperature.

It is well established that at elevated temperatures gaseous atoms in metal promote formation of gas bubbles [17–20]. Such temperatures are relevant for beryllium applications in fusion technology as plasma facing [21] and neutron multiplier material in tritium breeding blanket [22,23]. Above 500 °C vacancies are mobile in beryllium and gather into gas vacancy clusters giving rise to growth of gas bubbles [24]. Experiments on deuterium and tritium desorption have shown that deeper traps than vacancies should exist in beryllium, which are most probably gas bubbles, according to commonly accepted view [25–27]. It is, however, not clear presently whether hydrogen is trapped in the elastic field near gas

<sup>\*</sup> Corresponding author.

E-mail address: [dmitry.bachurin@kit.edu](mailto:dmitry.bachurin@kit.edu) (D.V. Bachurin).

bubble, at its surface or within bubble as molecule. Understanding of deep hydrogen trapping in irradiated beryllium is necessary for evaluation of residual tritium inventory accumulated in beryllium pebbles after the end of life of fusion reactor blanket. Such assessment is important for preventing burst release of trapped tritium due to plasma excursions to the first wall as well as for proper handling of radioactive wastes during decommissioning of the fusion blanket.

Therefore this work is devoted to one of the important mechanisms of hydrogen trapping on the surface of voids, in particular, to clarification of the effect of hydrogen interaction with pure beryllium surface including relaxation of the near surface interlayer distances and the change of surface energies causing modification of the shape of hydrogen covered voids.

Hydrogen interaction with metal surface is an important issue for development of catalysts, which are often composed of nanoparticles spread over a support material [28–30]. It is commonly assumed that a shape of nanoparticles is described in asymptotic limit of thermodynamical equilibrium by the Wulff construction and presence of gas results in a change of surface energy only. It should be, however, noted that the equilibrium surface concentration of gas atoms is different for various closed packed surfaces even within one bubble. Moreover, in case of not completely covered surfaces, their configurational entropy should be also taken into account.

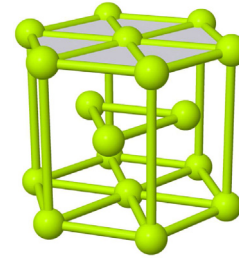
Both experimental studies [31,32] and previous *ab initio* calculations [33–36] show that the presence of hydrogen atoms considerably affects beryllium surface properties. Significant interplanar relaxation of the outermost atomic layers accompanied with the change of the structural and energetic characteristics occurs with increase of hydrogen coverage [36–45]. However, majority of the available *ab initio* studies are considering basal and prismatic type I surfaces only. In order to investigate the effect of hydrogen isotopes on the equilibrium shape of bubbles, information related to the energetics of other principal hcp beryllium surfaces with and without hydrogen is necessary.

In this paper, we start with *ab initio* study of critical hydrogen coverages on five principal beryllium surfaces. Then we consider effect of hydrogen concentration on surface energies and interplanar relaxation of the outermost surface layers. These results are used for construction of the equilibrium shape of voids covered with hydrogen. Two cases are considered: the same and different hydrogen concentration at different surfaces. Thereafter we compare our calculated equilibrium shapes with available experimental results on neutron irradiation or hydrogen implantation.

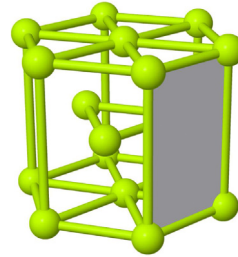
## 2. Computational methods

Static first principles calculations were performed using the Vienna *ab initio* simulation package (VASP) [46,47]. The pseudo potential based on the projector augmented wave (PAW) method was used to describe the interactions between ions and electrons. The generalized gradient approximation (GGA) of Perdew and Wang [48] was employed for calculation of the exchange correlation energy. Corresponding standard pseudopotentials for beryllium (with two valence electrons) and hydrogen were taken from the VASP library [49,50].

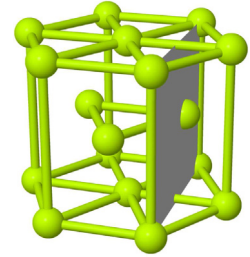
The effect of hydrogen on surface energies was investigated for five principal close packed beryllium planes: basal (0001), prismatic type I ( $1\bar{1}00$ ) and prismatic type II ( $2\bar{1}\bar{1}0$ ), pyramidal type I ( $1\bar{1}01$ ) and pyramidal type II ( $2\bar{1}\bar{1}2$ ) (see Fig. 1). Prismatic type I and pyramidal type I surfaces can be terminated in two possible ways. We have considered only the most stable and energetically favorable "short" termination as suggested in Refs. [39,44]. As far as



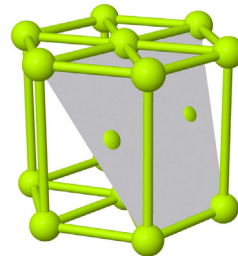
basal  
(0001)



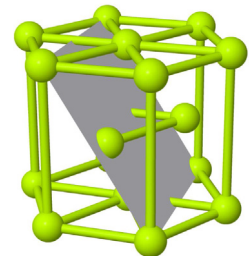
prismatic type I  
( $1\bar{1}00$ )



prismatic type II  
( $2\bar{1}\bar{1}0$ )



pyramidal type I  
( $1\bar{1}01$ )



pyramidal type II  
( $2\bar{1}\bar{1}2$ )

periodical boundary conditions are implied by VASP, an empty space of 17–23 Å (equivalent to four atomic layers) should be introduced into the simulation cell to avoid interaction between the top and the bottom of crystal bounded by closed packed planes being studied. The volume and the shape of the simulation cell were fixed, while no restrictions on the relaxation of atoms were imposed. The optimized lattice constants for bulk material were  $a = 2.265\text{Å}$  and  $c = 3.562\text{Å}$ . A Fermi smearing of 0.2 eV and the cut off energy of the plane waves of 450 eV were chosen. The tolerance for electronic self consistency step was set to be 0.01 eV and for ionic relaxation was stopped when forces were smaller than 0.01 eV/Å. The  $k$  point mesh was different for crystallographic non equivalent surfaces and presented in Table 1. The atomic structures were visualized using the program Jmol [51].

The surface area of the simulation cell was chosen large enough to avoid interaction of hydrogen with its periodical images at low hydrogen concentrations. At high hydrogen coverage such interactions are inevitable corresponding to the case of an infinite surface (see Table 1). Initial configurations for various coverages were constructed by addition of hydrogen atoms placed pairwise

**Table 1**

Configurations used in this work.  $N_{\text{Be}}$  is the number of beryllium atoms in the slab. The fourth column indicates the number of beryllium atomic layers perpendicular to the free surface.  $N_{\text{H}}^{100\%}$  is the number of hydrogen atoms corresponding to 100% of coverage.  $E_s^{0\%}$  and  $E_s^{100\%}$  in  $\text{J}/\text{m}^2$  are the energies of hydrogen-free and 100% covered beryllium surfaces, respectively. Two surfaces (20 $\bar{2}$ 1) and (21 $\bar{3}$ 0) denoted with symbol (\*) were studied at 0% hydrogen coverage only and were not used in construction of Wulff polyhedra.

| Surface           | cell size             | $N_{\text{Be}}$ | Be layers | $N_{\text{H}}^{100\%}$ | $k$ -points             | $E_s^{0\%}$ | $E_s^{100\%}$ |
|-------------------|-----------------------|-----------------|-----------|------------------------|-------------------------|-------------|---------------|
| (0001)            | $3 \times 3 \times 4$ | 72              | 8         | 9                      | $18 \times 18 \times 5$ | 1.71        | 1.64          |
| (1 $\bar{1}$ 00)  | $2 \times 3 \times 6$ | 72              | 12        | 12                     | $15 \times 5 \times 14$ | 1.80        | 1.53          |
| (2 $\bar{1}$ 10)  | $3 \times 3 \times 3$ | 108             | 6         | 18                     | $8 \times 9 \times 10$  | 2.02        | 1.88          |
| (1 $\bar{1}$ 01)  | $3 \times 2 \times 6$ | 72              | 12        | 12                     | $5 \times 15 \times 12$ | 1.83        | 1.08          |
| (2 $\bar{1}$ 12)  | $3 \times 2 \times 4$ | 96              | 8         | 24                     | $8 \times 11 \times 15$ | 2.40        | 0.76          |
| (20 $\bar{2}$ 1)* | $3 \times 1 \times 1$ | 48              | –         | –                      | $3 \times 9 \times 16$  | 1.81        | –             |
| (21 $\bar{1}$ )   |                       |                 |           |                        |                         |             |               |

on both free surfaces at the equivalent minimum energy sites: hcp site for basal plane; bridge site at the surface "ridge" for prismatic type I and II and pyramidal type II planes; a middle of triangle formed by two beryllium atoms at the surface "ridge" and one atom at the surface "valley" (for details see Ref. [34]). The configurations were constructed by sequential addition of hydrogen atoms to existing hydrogen rows, which generally may not correspond to the global minimum energy state at given coverage. More extended search performed for basal plane has shown that ground state can deviate by 0.1  $\text{J}/\text{m}^2$  from the value obtained by sequential addition (see Section 3.2).

The surface energy of beryllium slab with  $n$  hydrogen atoms referred to the free surface area,  $E_s$ , was defined as

$$E_s = \frac{1}{2S} \left( E_{\text{total}}^{\text{Be}+n\text{H}} - E_{\text{coh}}^{\text{Be}} \cdot N^{\text{Be}} - nE^{\text{H}} \right), \quad (1)$$

where  $E_{\text{total}}^{\text{Be}+n\text{H}}$  is the total energy of the system with  $n$  hydrogen atoms;  $E_{\text{coh}}^{\text{Be}} = 2.2367$  eV is the cohesive energy per beryllium atom in the bulk;  $N^{\text{Be}}$  is the number of beryllium atoms in the slab;  $E^{\text{H}} = 3.3590$  eV is the energy of one hydrogen atom in  $\text{H}_2$  molecule;  $S$  is the surface area of the slab. Factor two in Eq. (1) corresponds to the fact that the equivalent hydrogen configurations were prepared on both slab surfaces.

The adsorption energy of hydrogen (per one atom) with beryllium slab was calculated as

$$E_a = \frac{1}{n} \left( E_{\text{total}}^{\text{Be}+n\text{H}} - E_{\text{total}}^{\text{Be}} - nE^{\text{H}} \right), \quad (2)$$

where  $E_{\text{total}}^{\text{Be}}$  is the total energy of the beryllium slab without hydrogen. The value of the adsorption energy shows how strong hydrogen atoms are bound with beryllium surface. It should be noted that adsorption energy depends on particular distribution of hydrogen atoms on the surface.

Equilibrium shapes of voids were calculated using home made code and visualized with Jmol [51].

## 3. Results

### 3.1. Critical hydrogen coverage

Our *ab initio* molecular dynamics tests have shown an existence of an upper limit for hydrogen coverage on beryllium surfaces. At this coverage, named hereafter critical, no more hydrogen can be adsorbed from molecular hydrogen gas phase. Our *ab initio* molecular dynamics runs confirmed that at least two empty adjacent

adsorption sites are necessary for dissociative adsorption of diatomic molecule. This fact is in accordance with Langmuirian picture [52] which was recently reassessed in Ref. [53]. At critical coverage, there are no free adjacent adsorption sites, so that hydrogen molecule adsorption is suppressed. For the case of atomic hydrogen adsorption at such coverages, hydrogen atom adsorbing in the direct neighborhood of another pre adsorbed hydrogen will desorb as a molecule [54]. This process will result in reduction of hydrogen coverage. Therefore, the critical coverage is a theoretical upper limit (referred as 100%) which could be reached in both molecular and atomic hydrogen adsorption processes.

For basal surface the critical coverage corresponds to one hydrogen atom per beryllium surface atom (or one hydrogen per surface unit cell). The critical hydrogen coverages were calculated for other surfaces by placing hydrogen at different adsorption sites and performing static *ab initio* relaxations. Thus, the following critical surface coverages per surface unit cell were obtained: one hydrogen atom on basal plane; two hydrogen atoms on prismatic type I, type II and pyramidal type I planes; four hydrogen atoms on pyramidal type II plane (see Table 1).

Fig. 2 presents configurations with critical (100%) hydrogen coverage after relaxation. For all studied surfaces at higher coverages hydrogen prefers to be two fold coordinated with beryllium surface atoms in contrast to lower coverages, where hydrogen is three fold coordinated. Configurations with the intermediate hydrogen coverages (not presented here) are the mixture of both coordinations. Atop positions for hydrogen were not observed for any of the hcp beryllium surfaces.

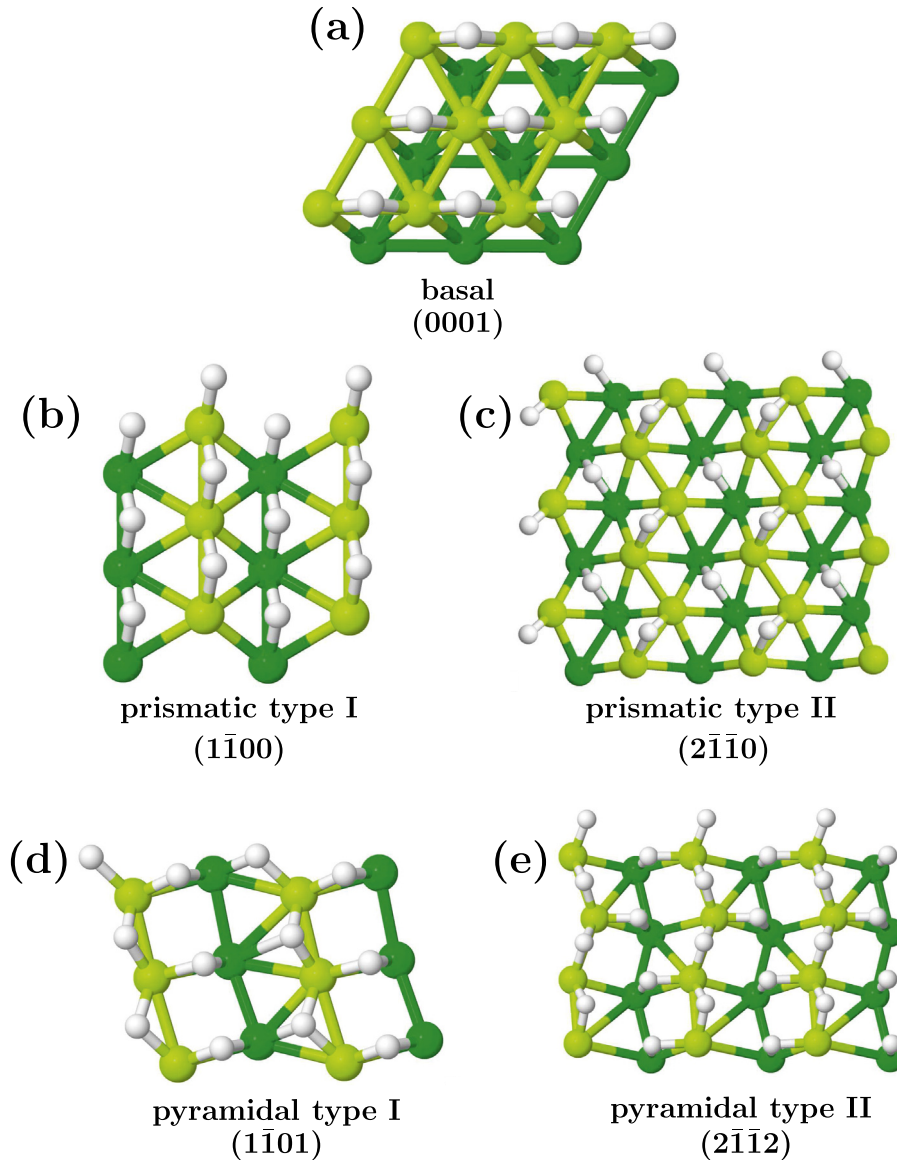
The results on single hydrogen atom adsorption for the principal close packed beryllium surfaces were presented in Ref. [34]. Here we discuss hydrogen adsorption at higher coverages.

**Basal.** At high coverage the bridge position is the most energetically favorable adsorption site (see Fig. 2a), although at low coverage it corresponds to a saddle point between hcp and fcc sites [34]. The length of the H–Be bond is 1.47 Å. At 100% coverage the hcp and fcc sites do not correspond to the global energy minima anymore. For example, the energy difference of the fcc and the bridge sites of the fully covered surface is as low as 0.22  $\text{J}/\text{m}^2$ . The distance between the first neighboring hydrogen atoms is 2.27 Å.

**Prismatic type I.** At critical coverage, the stable hydrogen adsorption sites are along the surface "ridge" and "valley" as illustrated in Fig. 2b. The length of the H–Be bond is of about 1.52 Å. All hydrogen atoms are located at bridge positions. The first neighboring hydrogen atoms are at the distance of 2.27 Å along the surface "ridge" or surface "valley".

**Prismatic type II.** Hydrogen atoms can be located at bridge positions along surface ridges and valleys as shown in Fig. 2c, which is similar to stable hydrogen sites of single atom [34]. The length of the H–Be bonds are 1.47 Å for surface "ridge" and 1.71 Å for surface "valley" similar to those found for single hydrogen atom. The distance between the first neighboring hydrogen atoms located at the surface "ridge" and surface "valley" is 2.74 Å. However, our calculations show that different hydrogen occupations of the  $3 \times 3$  surface leads to quite different results: one configuration with 9 hydrogen atoms (3 in the valleys and 6 on the ridges) appears to be stable, while another one (6 in the valleys and 3 on the ridges) demonstrate surface reconstruction. Further increase of hydrogen coverage (6 in the valleys and 6 on the ridges) results in the formation of  $\text{BeH}_2$  chains detaching from the surface during relaxation.

**Pyramidal type I.** At critical coverage half of the hydrogen atoms is located at bridge sites, while the other half is three fold coordinated with beryllium surface atoms (see Fig. 2d). The length of the H–Be bonds varies from 1.40 to 1.52 Å. Note, that both stable sites found for a single hydrogen atom were three fold



coordinated with beryllium atoms [34]. The distance between the nearest neighbor hydrogen atoms is 2.10 Å.

**Pyramidal type II.** All stable adsorption sites are bridge (two fold coordinated) positions with the bond lengths in the range of 1.41 to 1.45 Å. Fig. 2e demonstrates certain asymmetry in the positions of hydrogen atoms along the surface "valley". The first neighboring hydrogen atoms are located at the distance of 2.06 Å along the surface "ridge" and surface "valley".

### 3.2. Effect of hydrogen on beryllium surface energies

The effect of sequential addition of hydrogen atoms on the energies of five principal beryllium surfaces is presented in Fig. 3a. The following general trend is obvious: the surface energy first reduces, passes through the minimum and thereafter grows with the increase of hydrogen coverage. Thus, from a certain concentration, which is different on crystallographic non equivalent planes, further hydrogen adsorption on the free surfaces is

energetically less favorable. The energy of all considered beryllium surfaces covered with hydrogen atoms is always smaller than that of the corresponding clean surface. The energies of prismatic type I and pyramidal type I surfaces at zero coverage are almost equal, but they differ by 0.4 J/m<sup>2</sup> in the case of critical coverage. The presence of hydrogen changes drastically the energy of pyramidal type II surface from 2.4 down to 0.8 J/m<sup>2</sup>, i.e. the most unfavorable plane turns out to be the most favorable one at the coverage above 35%, while the energy of basal surface is 0.4–0.8 J/m<sup>2</sup> higher. In contrast to other surfaces, the energy of prismatic type II surface changes very insignificantly, in the range of 0.2 J/m<sup>2</sup> only.

Fig. 3b demonstrates the difference between the surface energies of configurations obtained via sequential addition of hydrogen atoms to existing hydrogen rows as well as some other alternative configurations obtained by more extensive ground state search for given coverages. As seen, the energy of basal plane can vary in the range of approximately 0.1 J/m<sup>2</sup>. The highest scattering of the values occurs near the energy minimum of 30–45% of

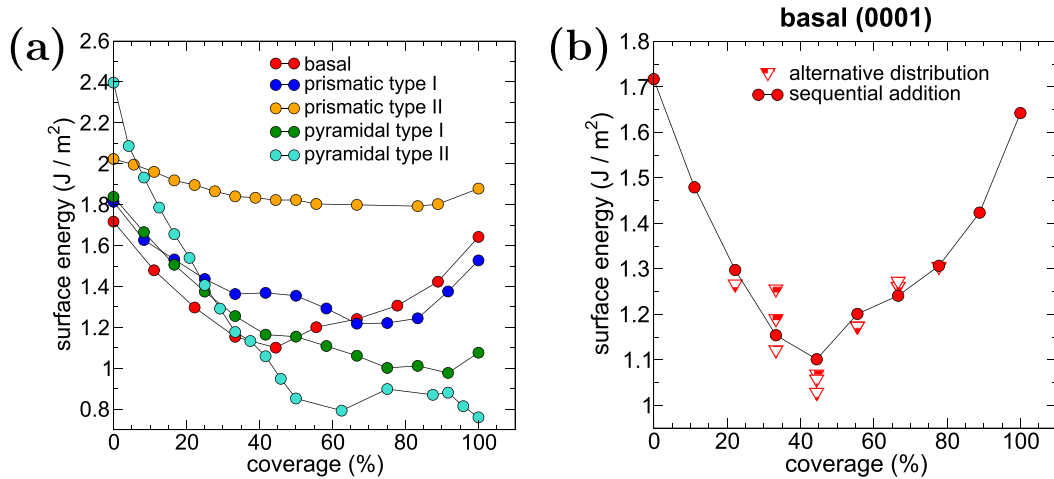


**Fig. 3.** (a) Surface energy of five principal beryllium planes as a function of hydrogen coverage. (b) A comparison of the surface energy of basal plane with sequential addition of hydrogen atoms and alternative hydrogen distributions. Zero coverage corresponds to the energy of beryllium surface without hydrogen atoms. Lines connecting the data points are guides to the eye.

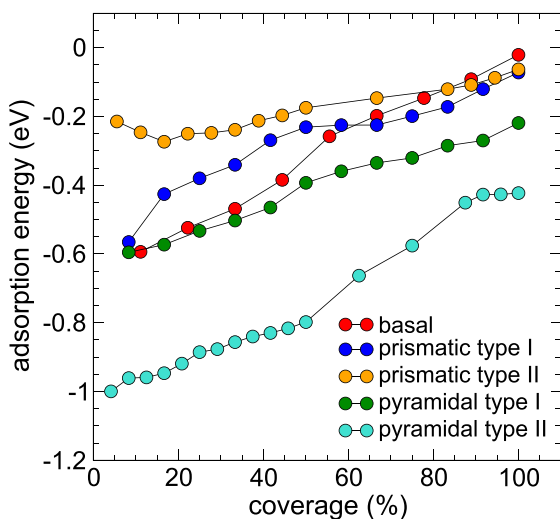
hydrogen coverage. It can be roughly assumed that similar deviation can be expected for the surface energies of other principal beryllium surfaces.

Fig. 4 illustrates tendency to roughly linear increase of adsorption energy (per one hydrogen atom) with hydrogen coverage for all studied beryllium surfaces. The lower the adsorption energy, the stronger hydrogen atoms are bound to beryllium surface. That is, hydrogen atoms on basal, prismatic type I and II surfaces are weakly bound at high coverages and desorption process from these surfaces supposed to occur easier and at temperatures lower than those from pyramidal type I and II.

### 3.3. Effect of hydrogen on interplanar relaxation

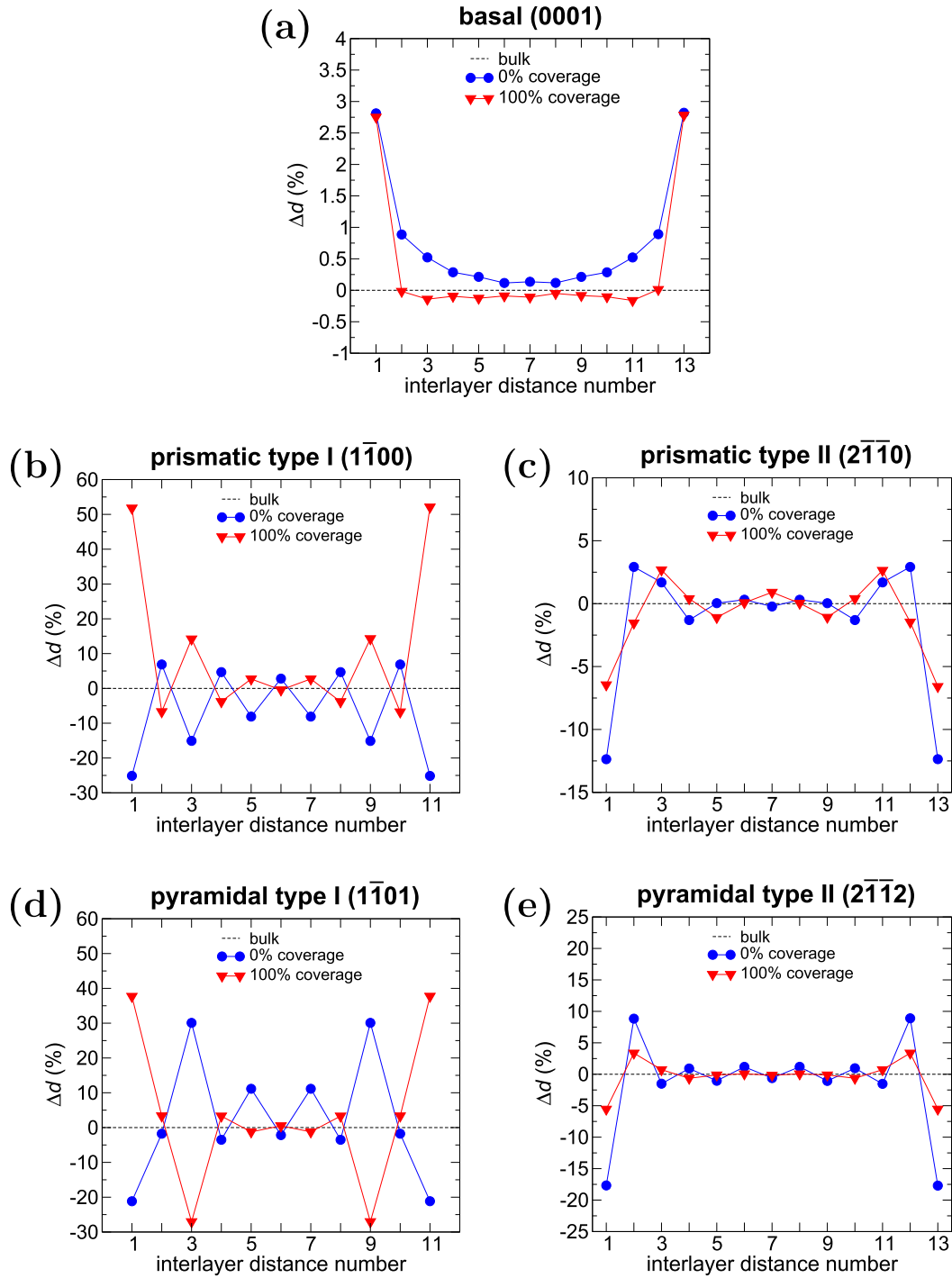
Fig. 5 demonstrates how the presence of hydrogen on beryllium surfaces changes the relaxation pattern of interplanar distances of outermost surface layers at critical coverage in comparison with clean beryllium surface. As shown previously [34], clean beryllium

slab with 10–14 layers exhibits in the middle nearly the same lattice constant as bulk material. At 100% coverage only the top layer of basal plane shows noticeable expansion, while the interplanar spacings for all other inner atomic planes are very close to the ideal hcp lattice value (see Fig. 5a). Adsorption of hydrogen slightly reduces the expansion of the first interplanar distance, while the other distances become very close to the bulk value. For prismatic type I and pyramidal type I surfaces, an oscillatory relaxation (interchanging stretching and compression between layers) takes place. Moreover, the compression (tension) of interlayer distances without hydrogen is replaced by the tension (compression) at critical hydrogen coverage as shown in Fig. 5b and d. Expansion of the "short" interlayer distances  $d_{12}$ ,  $d_{34}$ ,  $d_{56}$ , ... and contraction of the "long" distances  $d_{23}$ ,  $d_{45}$ ,  $d_{67}$ , ... is observed for prismatic type I surface at 100% coverage in contrast to the clean surface. In addition, the topmost surface layer demonstrate very significant relaxation over 50% for prismatic type I and around 40% for pyramidal type I surfaces. In general, the short terminated distances relax more notably than the "long" ones. Tension of the topmost short terminated distance  $d_{12}$  takes place, while other "short" distances  $d_{34}$  and  $d_{56}$  are under contraction for pyramidal type I surface which differs from the behavior of prismatic type I surface as seen in Fig. 5b and d. The percentage relaxation of the topmost layer of basal surface is approximately one order of magnitude lower than that for other studied beryllium surfaces. It is worth noting that the relaxation of the layers nearest to the surface is larger than that of the layers in the center of the slab. The relaxation patterns of prismatic type II and pyramidal type II surfaces at critical coverage and without hydrogen are relatively similar (see Fig. 5c and e).



### 3.4. Effect of hydrogen on equilibrium shape of voids in beryllium

Knowledge of the orientation dependence of the surface energy allows us to determine the equilibrium shape of a crystal or a void. This procedure is known as a Gibbs Wulff construction [55,56], which consist in minimization of the total surface free energy associated with the different surfaces. The geometry of the Wulff polyhedron follows the simple rule so that the distance from its centre to each face is proportional to surface energy of this face. Thus, the lower is the energy of the surface, the larger is its area in the Wulff polyhedron and vice versa.



### 3.4.1. Same hydrogen concentration on crystallographic non equivalent surfaces

First, we have performed classical Gibbs Wulff construction assuming that hydrogen concentrations are the same on different beryllium surfaces. Although the latter assumption might not be valid in general case, we used it here as a first approximation, which will be corrected in Section 3.4.2. Fig. 6 illustrates the computed equilibrium shape of a void in hcp beryllium single crystal without

hydrogen (0% of coverage), which is composed mainly of basal, prismatic type I and pyramidal type I faces. Since hydrogen readily adsorbs on beryllium surface up to critical coverage decreasing surface energy, notable change of equilibrium shape of void is expected especially at higher hydrogen coverages. A full disappearance of prismatic type II, a slight decrease of prismatic type I and an increase of the fraction of pyramidal type I facets are seen at 17% hydrogen coverage. Further increase of hydrogen concentration

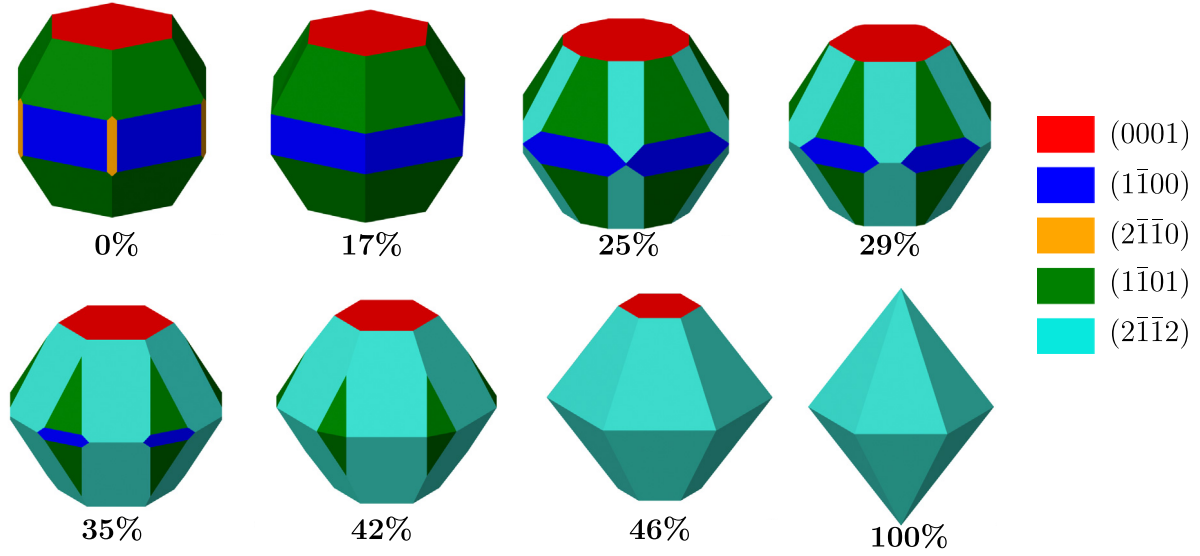


**Fig. 6.** Three-dimensional equilibrium shape of void in hcp beryllium single crystal as a function of hydrogen coverage (shown below) calculated with the assumption that hydrogen concentration is the same on all beryllium surfaces.

leads to a significant increase of the fraction of pyramidal type II facet. At 46% coverage the void is faceted with basal and pyramidal type II planes, while at critical coverage only pyramidal type II facets are present.

The dependence of the area of different hcp planes in the Wulff polyhedra on hydrogen concentration is shown in Fig. 7. The surface energy of the intermediate points were computed via fitting the curves in Fig. 3. Calculation of the area was performed with the assumption that the volume of polyhedron remains constant. As clearly seen, an increase of the area of one face is accompanied by a decrease of the area of another one. At hydrogen coverages lower than 12% Wulff polyhedra consist of mainly basal, prismatic type I and pyramidal type I facets. A significant growth of area of pyramidal type II facet is observed in the range of 12–40% of hydrogen coverage. Pyramidal type II facets dominate at concentrations higher than 40%. Note, that prismatic type II facet disappears

already at 2% of hydrogen coverage. At high coverage in the range between 75% and 95% there is an increase of area of pyramidal type I facets with the simultaneous reduction of the area of basal and pyramidal type II facets. At coverage higher than 96% Wulff polyhedra consist of one type of facets (pyramidal type II).

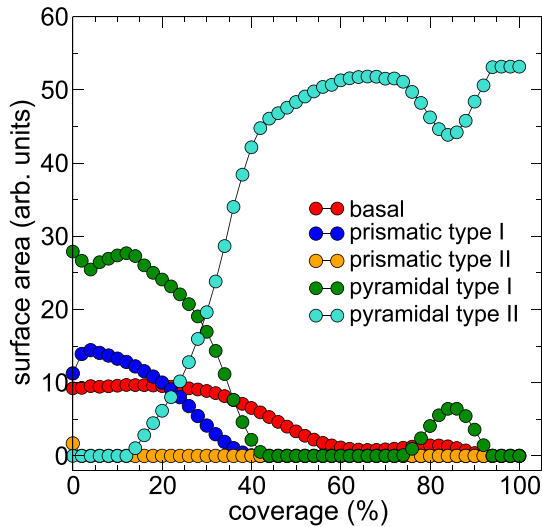
### 3.4.2. Different hydrogen concentration on crystallographic non equivalent surfaces

In this section we derive a generalization of the Gibbs Wulff construction for the case of different hydrogen coverages on crystallographic non equivalent surfaces. If we consider equilibrium of hydrogen adsorbed at void facets with hydrogen gas within a void, hydrogen coverage on non equivalent void facets will be different due to various adsorption and desorption barriers specific for each crystallographic plane. This is valid also for hydrogen dissolved in the bulk being in equilibrium with hydrogen on the void surfaces. Different surface coverages in this case are due to different energies of hydrogen atoms on various surfaces. Hence, the case considered in this section reflects real physical phenomenon. The equilibrium shape of growing single crystal or void in otherwise perfect single crystal is determined by the minimization of its Gibbs free energy, which for the case of gas covered bubble can be written as:

$$\Delta G = \sum_i (\gamma_i A_i - TS_i). \quad (3)$$

Here  $\gamma_i$  is the surface energy,  $A_i$  is surface area of  $i$ th face,  $T$  and  $S_i$  are temperature and entropy, respectively. In this case the surface energy and entropy are functions of hydrogen surface coverage  $c_i$  on  $i$ th face. The summation runs over all void faces and we assume that hydrogen coverage can be different for faces of different orientations. Accounting for configurational entropy allowed us to include temperature dependence of Gibbs free energy and, as a consequence, the effect of temperature on the equilibrium shape of void or nanoparticle. This effect was missing in the classical Gibbs Wulff approach considered in the previous section.

Let us assume that each void contains definite number of hydrogen atoms  $N_0 = \sum_i N_i$ , where the number of hydrogen atoms on each face  $N_i$  is related to the hydrogen surface coverage as



$$c_i = \frac{\sigma_i}{A_i} N_i. \quad (4)$$

Here  $\sigma_i$  is a surface area per one adsorption site on the  $i$  th face. Our calculations have shown that the critical hydrogen coverage per unit cell is: one hydrogen atom on basal plane; two hydrogen atoms on prismatic type I, type II and pyramidal type I planes; four hydrogen atoms on pyramidal type II plane (see Table 1). Despite the fact that multiple adsorption sites are available, they cannot be occupied simultaneously.

The minimization of free energy (3) should be performed taking into account the conservation of void volume  $V_0$  and the number of hydrogen atoms  $N_0$ . This can be done using the method of Lagrange multipliers by minimizing auxiliary function:

$$\Omega(A) = \sum_i [\gamma_i(c_i) A_i - T S_i(c_i)] - \lambda \left( \sum_i h_i A_i - 3V_0 \right) - \mu \left( \sum_i N_i - N_0 \right). \quad (5)$$

Here  $h_i$  is the height of the pyramid with base on the face, which is proportional to the surface energy of the face;  $\lambda$  is the Lagrange multiple defining only the size of a crystal or a void, but not its shape;  $\mu$  is the Lagrange multiple associated with the free energy change per hydrogen atom (equivalent to chemical potential). The term after  $\lambda$  implies volume conservation, while the term after  $\mu$  takes into account conservation of the number of hydrogen atoms.

Differentiating (5) with respect to  $N_i$  gives

$$\frac{\partial \Omega(A)}{\partial N_i} = \left[ \frac{\partial \gamma_i}{\partial c_i} A_i - T \frac{\partial S_i}{\partial c_i} \right] \frac{\partial c_i}{\partial N_i} - \mu = 0. \quad (6)$$

Using relation (4), we obtain

$$\frac{\partial c_i}{\partial N_i} = \frac{\sigma_i}{A_i}. \quad (7)$$

Substitution of (7) in (6) gives the expression for  $\mu$

$$\mu = \frac{\partial \gamma_i}{\partial c_i} \sigma_i - T \frac{\partial S_i}{\partial c_i} \frac{\sigma_i}{A_i}. \quad (8)$$

The following equation for configurational entropy for the  $i$  th face can be used:

$$S_i(c_i) = k_B \frac{A_i}{\sigma_i} [(1 - c_i) \ln(1 - c_i) + c_i \ln c_i], \quad (9)$$

where  $k_B$  is Boltzmann constant. Differentiating of (9) with respect to  $c_i$ , we obtain

$$\frac{\partial S_i}{\partial c_i} = k_B \frac{A_i}{\sigma_i} \ln \left( \frac{1 - c_i}{c_i} \right). \quad (10)$$

Substitution of (10) in (8) gives us the final expression for the chemical potential

$$\mu = \frac{\partial \gamma_i}{\partial c_i} \sigma_i - k_B T \ln \left( \frac{1 - c_i}{c_i} \right). \quad (11)$$

Further, the determination of the equilibrium void shape was performed using the following steps:

1. With relation (11) we evaluate the chemical potential for different surfaces as a function of hydrogen coverage. Analytical expressions for  $\gamma_i(c_i)$  were obtained by fitting the curves in Fig. 3a. The dependencies  $\mu(c_i)$  are presented in Fig. 8 for two different temperatures. Such large range of temperatures from

0.1 to 1500 K was chosen to demonstrate to what extent the chemical potential changes with temperature at given hydrogen coverage.

2. Assuming that chemical potential  $\mu$  in equilibrium is the same on all surfaces, we determine hydrogen concentrations  $c_i$  on different faces. As seen in Fig. 8, up to three different hydrogen concentrations can be referred to the same value of  $\mu$ . Each solution corresponds to different number of hydrogen atoms at the surface of void.
3. Using these concentrations  $c_i$  we calculate the surface energies from the fitted curves  $\gamma_i(c_i)$  and then perform construction of Voronoi polyhedra. The results are shown in Fig. 9 for two temperatures and five different values of chemical potential in the range from 0.8 to 0.8.

The shapes calculated with this method are quite different from those found with the use of conventional Gibbs–Wulff construction. However, for high hydrogen coverage both methods predict the same equilibrium shape of hydrogen covered void: the remaining small fraction of basal facet at 86% (shown in Fig. 9) fully disappears at 99.5% and Voronoi polyhedra consist of only pyramidal type II facets.

Fig. 9 confirms that both chemical potential and temperature influence the equilibrium shape of a hydrogen covered void. An increase of  $\mu$  results in a gradual disappearance of all facets with the exception of pyramidal type II ones. At high temperature of  $T = 1500$  K the shape of Voronoi polyhedra does not change so distinctly as at  $T = 0.1$  K with variation of chemical potential. Notice also, that our model predicts practically identical polyhedra for  $\mu \geq 0.4$  regardless of the temperature.

The intermediate configurations with the coverages in the range of 10–95% used for fitting did not necessarily correspond to the absolute energy minimum, therefore the shape the Wulff polyhedra may deviate from those displayed in Fig. 6. However, according to our evaluation the energy of basal surface can vary only within 0.1 J/m<sup>2</sup> depending on the hydrogen distribution on the surface (see Fig. 3b). Therefore, only minor changes in equilibrium shape of voids associated with an increase or decrease of the area of some of the facets may occur.

## 4. Discussion

### 4.1. Critical hydrogen coverage

Our calculations show that the stable hydrogen adsorption sites at high coverage can noticeably differ from those at lower coverage. For basal surface, hydrogen atoms prefer to occupy bridge sites and to be two fold coordinated at critical coverage (see Fig. 2a). Early first principles simulations [57,58] have revealed that the bridge position (above the middle of the Be–Be bond) on basal plane is a stable adsorption site for one hydrogen atom at 0 K in the smallest  $1 \times 1$  computational cell corresponding to the 100% coverage. In this work stable bridge adsorption sites were repeatedly reproduced with larger simulation cells at high hydrogen coverages.

Allouche reported a possibility of higher hydrogen coverage than that found in our work on Be(0001) surface [33]. Namely, the full coverage of the  $3 \times 3$  cell is achieved when 12 hydrogen atoms are adsorbed above 9 beryllium surface atoms. Fig. 3c from Ref. [33] shows that most of the hydrogen atoms prefer two fold coordinated bridge position building a kind of disordered Be–H half rings at the surface similar to BeH<sub>2</sub> molecular polymer chains [59,60]. In our previous work [34] we made an attempt to place two hydrogen atoms per one beryllium atom (corresponding to 18 hydrogen per 9 beryllium atoms for the  $3 \times 3$  cell) on basal plane. This attempt, however, ended with athermal desorption of several hydrogen

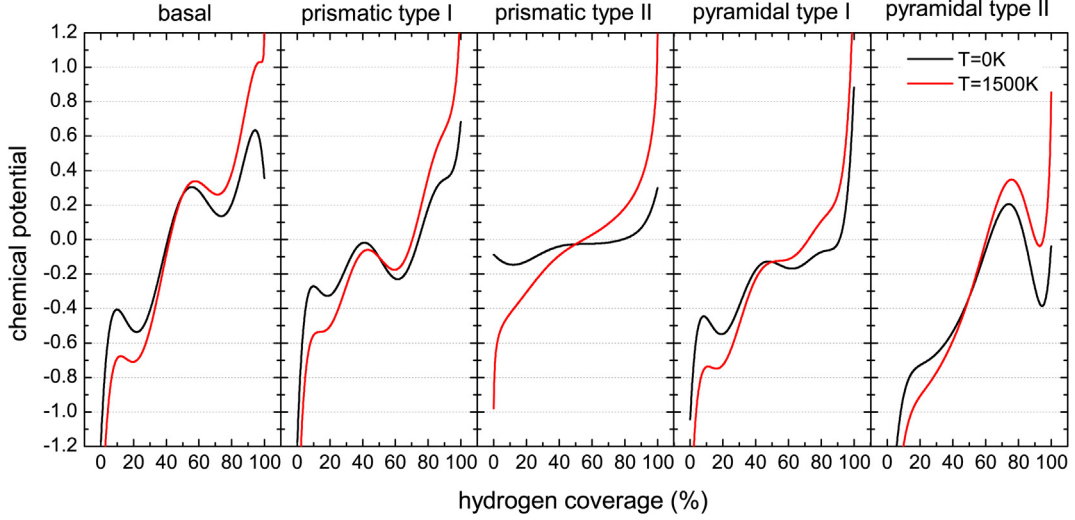
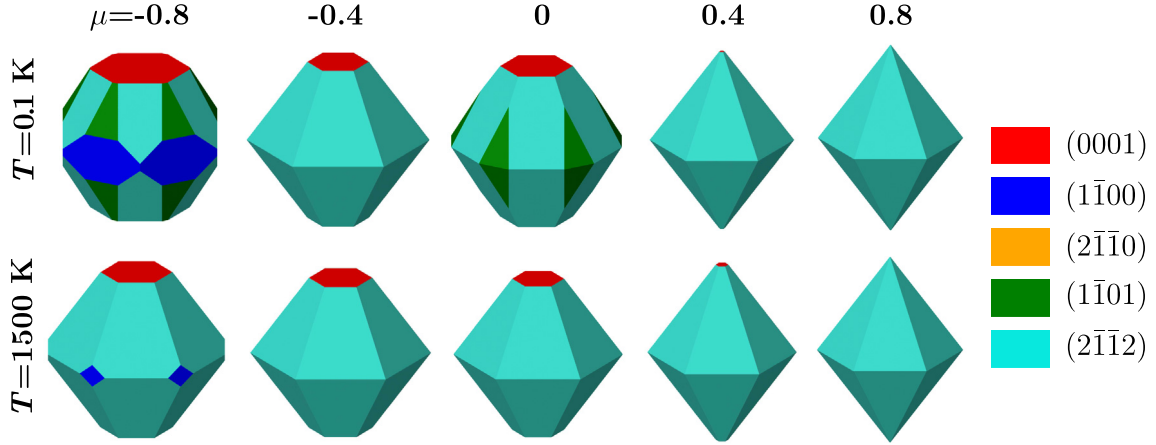


Fig. 8. Chemical potential calculated using expression (8) as a function of hydrogen coverage at two different temperatures.



molecules, while no desorption occurred at the coverage of one hydrogen per one surface beryllium atom showing formation of similar distorted Be–H half rings. We found that at the coverage above one hydrogen per beryllium surface atom severe surface reconstruction takes place.

Our results suggest that the critical coverage, above which no molecular adsorption is possible, cannot be increased by atomic hydrogen adsorption alone. Adsorption of atomic hydrogen occurs without barrier, but after that hydrogen molecule is formed readily and desorbs from the surface thus decreasing the surface coverage. The only process which can increase hydrogen coverage above critical value is diffusion of hydrogen from the bulk. Probably, the highest coverage can be reached with two hydrogen atoms per one beryllium atom corresponding to formation of complete  $\text{BeH}_2$  chains. This analysis shows that our findings are in fact complementary to the results of Allouche [33] although do not coincide in all details. In this work we found similar trend in hydrogen adsorption energy behavior with increase of hydrogen coverage.

We are not aware of other theoretical works devoted to the calculation of surface energies of beryllium with hydrogen. Even calculations for clean planes other than basal one (mainly prismatic type I plane) are very limited [38–40,42,44,45,61]. However, our

findings can be indirectly compared with the work of Udagawa et al. [62]. They have revealed a noticeable reduction of the surface energy for hcp basal and prismatic type I planes with an increase of hydrogen concentration in solid solution in another hcp metal, zirconium. Note, the change of the surface energy is related not only to presence of hydrogen on the surfaces, but to some extent to relaxation of interlayer distances.

#### 4.2. Relaxation of surface layers

Feibelman et al. [36,58,63] studied the relaxation of outermost surface layers of basal plane at monolayer hydrogen coverage. The smallest  $1 \times 1$  simulation cell was used, where one hydrogen atom per beryllium surface atom on basal surface corresponds already to the monolayer (100%) coverage. The first surface layer was found to be compressed with  $d_{12} \approx 0.27\%$  of the bulk value [58], although it was stretched showing 10 times higher value of  $d_{12} = 2.6\%$  in work [36]. Unfortunately, it is difficult to explain the difference of one order of magnitude (and even the opposite sign) between the results obtained by the same author within slightly different frameworks. However, the latter result is in a good agreement with our findings (see Fig. 5a). We are not aware of the works, where the

relaxation of outermost surface layers of other principal close packed beryllium surfaces at high hydrogen coverage was investigated.

Beryllium is known for large relaxation of the interplanar distances near clean surface [36–45,61,64]. The addition of hydrogen generally results in the reduction of the interplanar distances, although for prismatic type I and pyramidal type I planes the contraction of the first interplanar distance is replaced by even larger expansion.

Bavli et al. [65] argue that the inward relaxation of the top surface layer occurs due to the lower electron density at the surface in comparison with the bulk. In our case this is true for all surfaces except basal one. In order to validate the connection between the change of electron density and the relaxation of interlayer distances, we have performed calculations of integral charge density as a function of thickness for basal, prismatic type I and pyramidal type I surfaces. It was found that if the value of the integral charge density between atoms increases then the distance between layers decreases resulting in inward relaxation. This behavior can be rationalized in terms of nuclear charge screening. Increased charge density between atoms results in decrease of Coulomb repulsion between nuclei, i.e. their mutual attraction. Thus the rule of thumb in the case of surface layer relaxation can be formulated in the following form: the increase of electron density between atomic layers parallel to the surface results in contraction of the interlayer distance and vice versa.

#### 4.3. Equilibrium shape of hydrogen covered voids

Equilibrium shape of hcp crystals was studied thoroughly [28,65–69]. In this work we found similar topology of the Wulff polyhedron. The only difference from the cited works is the presence of a small fraction of prismatic type II face, which cuts an edge formed between two adjacent prismatic type I faces. We are aware of only one attempt to construct Wulff polyhedron for hcp beryllium crystal [69,70]. The form of the constructed polyhedron slightly differs from ours. Namely, the authors in the cited paper revealed the presence of  $\{20\bar{2}1\}$  facet, which cuts an edge between  $\{1\bar{1}00\}$  and  $\{1\bar{1}01\}$  planes and a small fraction of  $\{21\bar{3}0\}$  facet instead of  $\{2\bar{1}\bar{1}0\}$  in our case (for details see Ref. [70]).

Inspired by the comprehensive work of Tran [69,70], we have performed for completeness calculation of the energy of  $(20\bar{2}1)$  and  $(21\bar{3}0)$  surfaces. The data are presented in Table 1. The comparison shows that our results for the surfaces (1.81 J/m<sup>2</sup> for  $(20\bar{2}1)$  and 1.99 J/m<sup>2</sup> for  $(21\bar{3}0)$ ) are on average 0.1 J/m<sup>2</sup> lower than the corresponding values obtained by Tran and co workers, which is undoubtedly related to another set of simulation parameters used. The energies of  $(20\bar{2}1)$  and  $(21\bar{3}0)$  surfaces are very close to those for prismatic type I and type II planes, respectively. Analysis shows that  $(20\bar{2}1)$  surface does not result in a drastic change of equilibrium shape of void at 0% of coverage, while the ratio of  $(21\bar{3}0)$  surface is relative small. On this basis, we do not consider the effect of these two surfaces on the shape of Wulff polyhedra.

No attempts to study the change of the Wulff polyhedron topology for beryllium as a function of hydrogen coverage were made so far. However, somewhat similar calculations were carried out for rhenium nanoparticles covered with oxygen as well as nitrogen atoms [28]. The authors, using *ab initio* atomistic thermodynamics approach, have demonstrated that the equilibrium shape of rhenium particles significantly changes with both oxygen and nitrogen coverages (see Fig. 2 in Ref. [28]).

It is interesting to compare our simulation results with experiments. Under neutron irradiation beryllium transmutes to helium

and tritium, with a ratio of helium to tritium concentration in the range of 10–200 depending on neutron spectrum [71]. The growth of helium bubbles in beryllium under neutron irradiation at elevated temperatures was extensively studied using optical [72,73] and transmission electron microscopy [24,74–76]. It is well established that helium bubbles have a shape of hexagonal prism with the base lying on basal plane (see, e.g. Refs. [24,76]). It was shown that the width to height ratio varies within 2–5 depending on the irradiation conditions. The side faces of the prism are assumed to be rectangular  $\{01\bar{1}0\}$  facets. Exactly this shape was not found in our calculations. The most similar shape is that at zero hydrogen coverage that shows the presence of pyramidal type I planes in contrast to helium bubbles. Nevertheless, in addition to regular prisms, some bubbles are truncated by one of the pyramidal planes instead of prismatic ones (see Fig. 5b in Ref. [76]) which were found as facets in our Gibbs Wulff construction.

It should be mentioned that in the neutron irradiation experiments helium bubbles contain at least one order of magnitude more helium than hydrogen isotopes. Much higher hydrogen concentrations can be reached in ion implantation experiments. For formation of faceted voids of different shape elongated along  $[0001]$  direction was observed after implantation with deuterium ions at 500 and 700 K [27]. Annealing at 500–600 °C for 15 min of beryllium implanted with hydrogen at temperature below 50 °C has revealed the elongated shape of voids along  $[0001]$  direction which were truncated by pyramidal planes from both ends (see Fig. 5a in Ref. [77]).

Thus, our model calculations predict a general trend of the faceting shape of void with increase of hydrogen surface coverage on its facets. The area of the most energetically favorable (without hydrogen) basal surface is decreasing until it disappears, while the area of the pyramidal type II plane is dominating at high hydrogen coverage. With increase of hydrogen concentration only the later surface survives while all other facets disappear completely (see Fig. 7). However, it fails to reproduce the exact shape of voids with hydrogen observed in experiments. The main reason for this behavior, in our opinion, is the kinetic nature of the process of void growth.

Recent work of Xu et al [78] shed some light on the kinetics of void formation in similar hcp metal, magnesium. Using the high resolution transmission electron microscopy, the authors observed void growth induced by electron irradiation. They found that the voids first grow into a plate like hexagonal shape on basal plane, followed by a gradual increase of the height of the prism. During the first stage the prism is truncated from the sides by pyramidal type I planes. Prismatic planes appear in the second stage of the growth. This work shows that the process of void growth under irradiation is essentially non equilibrium and is driven by anisotropic growth kinetics.

The above described experiment demonstrates that applicability of equilibrium methods depends on the ratio between the rates of surface diffusion and void growth. If surface diffusion is slower, the void shape is defined by kinetics of the growth process and can be far from the shape expected at equilibrium. Moreover, after the end of irradiation or annealing used in experiments we do not know how far this frozen stage is from the equilibrium. Increase of temperature affects the diffusion limited growth of void and decreases the time necessary to reach the equilibrium state. Hence, experiments performed at different temperatures sometimes report different faceting of the voids. For instance, bubbles with argon gas in hcp zinc after bombardment in heavy ion accelerator at 300 °C were bounded by basal, pyramidal type I and prismatic type I facets, while at lower temperature of 130 °C the dominating facets were basal and prismatic type I [66].

Another possible reason for discrepancy, namely different hydrogen coverage for different void facets, was tested in the present work. Although notable differences have been found with respect to the case of equal coverages reported in Ref. [35], the shape of void still differs from that observed in experiments.

The observed phenomenon of void faceting modification in the presence of hydrogen suggests a practical way of deliberate adjustment of nanoparticle morphology which is known to play an essential role in their catalytic activity. Catalyst particles grown on the substrate can be shaped in hydrogen or other gas atmosphere which affects surface energies and facilitates formation of certain facets. Similar process was studied in application to rhenium nanoparticles in oxygen and nitrogen environments [28].

## 5. Conclusions

In this paper we have studied the effect of hydrogen surface coverage on surface energy and relaxation of outermost atomic layers for five principal hcp beryllium surfaces (basal, prismatic type I and II, pyramidal type I and II). Equilibrium shapes of hydrogen covered voids in beryllium were determined assuming different hydrogen coverages on crystallographic non equivalent surfaces.

The main conclusions can be drawn as follows.

1. The critical hydrogen coverage above which hydrogen molecular adsorption from gas phase stops was determined for all studied beryllium surfaces. At this coverage hydrogen prefers to be two fold coordinated with beryllium atoms, i.e. occupies mainly the bridge site above the middle of Be–Be bond. Hydrogen bonding with two surface beryllium atoms resembles half of BeH<sub>2</sub> ring.
2. Adsorption of hydrogen on beryllium surface results in a significant reduction of surface energy for basal, prismatic type I and pyramidal type I and II surfaces, while the energy of prismatic type II surface changes only moderately. The latter has the same bridge like hydrogen adsorption positions for clean and pre covered surfaces.
3. At hydrogen coverage above ca. 40% pyramidal type II plane is the most energetically favorable, while the energies of other studied surfaces are noticeably higher.
4. Relaxation of outermost atomic layers covered with hydrogen considerably differs from that found for clean beryllium surfaces. Interchanging extension and compression between layers occurs for prismatic type I and pyramidal type I surfaces with and without hydrogen.
5. An equilibrium shape of hydrogen covered voids in beryllium was studied using generalized Gibbs Wulff construction accounting for different hydrogen coverages on crystallographic non equivalent surfaces. Voids without hydrogen are bounded with basal, prismatic type I and pyramidal type I planes with a small fraction of prismatic type II facets. Our model predicts drastic changes of faceting with hydrogen coverage so that at critical coverage all faces are pyramidal type II planes. Obtained results are partially consistent with the available experimental data.
6. Differences between the proposed model and experiments can be explained by the fact that no equilibrium was reached in experiments, while kinetic processes are responsible for the faceting of hydrogen covered voids formed under neutron irradiation or after thermal annealing.

## Acknowledgements

This work has been carried out within the framework of the

EUROfusion Consortium and has received funding from the Euratom research and training programme 2014–2018 under grant agreement No 633053. The views and opinions expressed herein do not necessarily reflect those of the European Commission. Computational resources were provided by the IFERC Computational Simulation Centre (Rokkasho, Japan) and the Steinbuch Centre for Computing (Karlsruhe, Germany). The authors are grateful to Dr. V. Borodin for his help in evaluation of the charge density profiles and fruitful discussions.

## References

- [1] T. Parsonage, Beryllium metal matrix composites for aerospace and commercial applications, *Mater Sci. Tech. Ser.* 16 (2000) 732–738.
- [2] Y. Wang, Y. Xiong, Effects of beryllium in Al–Si–Mg–Ti cast alloy, *Mat. Sci. Eng. A Struct.* 280 (2000) 124–127.
- [3] Z.H. Feng, X.J. Jiang, Y.K. Zhou, C.Q. Xia, S.X. Liang, R. Jing, X.Y. Zhang, M.Z. Ma, R.P. Liu, Influence of beryllium addition on the microstructural evolution and mechanical properties of Zr alloys, *Mater Des.* 65 (2015) 890–895.
- [4] J.M. Beeston, Beryllium metal as a neutron moderator and reflector material, *Nucl. Eng. Des.* 14 (1970) 445–474.
- [5] J.J. Hu, E. Rohm, M. Fichtner, Feasibility and performance of the mixture of MgH<sub>2</sub> and LiNH<sub>2</sub> (1:1) as a hydrogen-storage material, *Acta Mater.* 59 (2011) 5821–5831.
- [6] J. Zhang, G.Y. Zhou, G.R. Chen, M. Latroche, A. Percheron-Guegan, D. Sun, Relevance of hydrogen storage properties of ANi(3) intermetallics (A = La, Ce, Y) to the ANi(2) subunits in their crystal structures, *Acta Mater.* 56 (2008) 5388–5394.
- [7] M. Danaie, D. Mitlin, TEM analysis of the microstructure in TiF<sub>3</sub>-catalyzed and pure MgH<sub>2</sub> during the hydrogen storage cycling, *Acta Mater.* 60 (2012) 6441–6456.
- [8] W. Grochala, P.P. Edwards, Thermal decomposition of the non-interstitial hydrides for the storage and production of hydrogen, *Chem. Rev.* 104 (2004) 1283–1315.
- [9] A.D. Zdetsis, M.M. Sigalas, E.N. Koukaras, Ab initio theoretical investigation of beryllium and beryllium hydride nanoparticles and nanocrystals with implications for the corresponding infinite systems, *Phys. Chem. Chem. Phys.* 16 (2014) 14172–14182.
- [10] K. Sumida, M.R. Hill, S. Horike, A. Dailly, J.R. Long, Synthesis and hydrogen storage properties of Be-12(OH)(12)(1,3,5-benzenetribenzoate)(4), *J. Am. Chem. Soc.* 131 (2009) 15120–15121.
- [11] R. Shinde, M. Tayade, Remarkable hydrogen storage on beryllium oxide clusters: first-principles calculations, *J. Phys. Chem. C* 118 (2014) 17200–17204.
- [12] H. Lee, B. Huang, W.H. Duan, J. Ihm, Ab initio study of beryllium-decorated fullerenes for hydrogen storage, *J. Appl. Phys.* 107 (2010) 084304.
- [13] D.Y. Li, Y. Ouyang, J.F. Li, Y.Y. Sun, L. Chen, Hydrogen storage of beryllium adsorbed on graphene doping with boron: first-principles calculations, *Solid State Commun.* 152 (2012) 422–425.
- [14] L. Schlapbach, A. Züttel, Hydrogen-storage materials for mobile applications, *Nature* 414 (2001) 353–358.
- [15] Y. Fukai, *The Metal-Hydrogen System: Basic Bulk Properties*, in: Springer Series in Materials Science, Springer, 2005.
- [16] M.G. Ganchenkova, V.A. Borodin, R.M. Nieminen, Hydrogen in beryllium: solubility, transport, and trapping, *Phys. Rev. B* 79 (2009) 134101.
- [17] J.B. Condon, T. Schober, Hydrogen bubbles in metals, *J. Nucl. Mater* 207 (1993) 1–24.
- [18] P.B. Johnson, D.J. Mazey, Helium gas bubble lattices in face-centered-cubic metals, *Nature* 276 (1978) 595–596.
- [19] P.B. Johnson, D.J. Mazey, Gas-bubble superlattice formation in Bcc metals, *J. Nucl. Mater* 218 (1995) 273–288.
- [20] F.E. Lawson, P.B. Johnson, A temperature threshold for gas-bubble superlattice formation in molybdenum, *J. Nucl. Mater* 252 (1998) 34–42.
- [21] V. Barabash, R. Eaton, T. Hirai, I. Kupriyanov, G. Nikolaev, Z.H. Wang, X. Liu, M. Roedig, J. Linke, Summary of beryllium qualification activity for ITER first-wall applications, *Phys. Scr.* T145 (2011) 014007.
- [22] Y. Poitevin, L.V. Boccacini, M. Zmitko, I. Ricapito, J.F. Salavy, E. Diegele, F. Gabriel, E. Magnani, H. Neuberger, R. Lasser, L. Guerrini, Tritium breeder blankets design and technologies in Europe: development status of ITER Test Blanket Modules, test & qualification strategy and roadmap towards DEMO, *Fusion Eng. Des.* 85 (2010) 2340–2347.
- [23] P. Vladimirov, D. Bachurin, V. Borodin, V. Chakin, M. Ganchenkova, A. Fedorov, M. Klimenkov, I. Kupriyanov, A. Moeslang, M. Nakamichi, T. Shibayama, S. Van Til, M. Zmitko, Current status of beryllium materials for fusion blanket applications, *Fusion Sci. Technol.* 66 (2014) 28–37.
- [24] V.P. Chakin, Z.Y. Ostrovsky, Evolution of beryllium microstructure under high-dose neutron irradiation, *J. Nucl. Mater* 307 (2002) 657–663.
- [25] M. Reinelt, C. Linsmeier, Temperature programmed desorption of 1 keV deuterium implanted into clean beryllium, *Phys. Scr.* T128 (2007) 111–114.
- [26] V. Chakin, R. Rolli, A. Moeslang, M. Klimenkov, M. Kolb, P. Vladimirov, P. Kurinskiy, H.C. Schneider, S. van Til, A.J. Magielsen, M. Zmitko, Tritium

- release and retention properties of highly neutron-irradiated beryllium pebbles from HIDOBE-01 experiment, *J. Nucl. Mater* 442 (2013) S483–S489.
- [27] V.N. Chernikov, V.K. Alimov, A.V. Markin, A.E. Gorodetsky, S.L. Kanashenko, A.P. Zakharov, I.B. Kupriyanov, Gas-induced swelling of beryllium implanted with deuterium ions, *J. Nucl. Mater* 233 (1996) 860–864.
- [28] P. Kaghazchi, T. Jacob, Structure-activity relation of Re nanoparticles, *Phys. Rev. B* 86 (2012) 085434.
- [29] J.A. Enterkin, K.R. Poeppelmeier, L.D. Marks, Oriented catalytic platinum nanoparticles on high surface area strontium titanate nanocuboids, *Nano Lett.* 11 (2011) 993–997.
- [30] Q.-L. Zhu, Q. Xu, Immobilization of ultrafine metal nanoparticles to high-surface-area materials and their catalytic applications, *Chem* 1 (2016) 220–245.
- [31] K. Pohl, E.W. Plummer, Structure of the H-induced vacancy reconstruction of the (0001) surface of beryllium, *Phys. Rev. B* 59 (1999) R5324–R5327.
- [32] K. Pohl, E.W. Plummer, S.V. Hoffmann, P. Hofmann, Phase diagram of hydrogen on Be(0001) from reconstruction-induced surface core-level shifts, *Phys. Rev. B* 70 (2004) 235424.
- [33] A. Allouche, Density functional study of hydrogen adsorption on beryllium (0001), *Phys. Rev. B* 78 (2008) 085429.
- [34] D.V. Bachurin, P.V. Vladimirov, Ab initio study of hydrogen on beryllium surfaces, *Surf. Sci.* 641 (2015) 198–203.
- [35] D.V. Bachurin, P.V. Vladimirov, Simulation of hydrogen effect on equilibrium shape of gas bubbles in beryllium, *Fusion Eng. Des.* 109 (2016) 1432–1436.
- [36] R. Stumpf, P.J. Feibelman, Interaction of hydrogen with the Be(0001) surface, *Phys. Rev. B* 51 (1995) 13748–13759.
- [37] A. Antonelli, S.N. Khanna, P. Jena, Interplanar relaxation at the (0001) surface of Be, *Surf. Sci.* 289 (1993) L614–L616.
- [38] R. Stumpf, J.B. Hannon, P.J. Feibelman, E.W. Plummer, The unusual properties of beryllium surfaces, in: E. Bertel, M. Donath (Eds.), *Electronic Surface and Interface States on Metallic Systems*, World Scientific, Singapore, 1995, p. 151.
- [39] P. Hofmann, K. Pohl, R. Stumpf, E.W. Plummer, Geometric structure of Be(10 $\bar{1}$ 0), *Phys. Rev. B* 53 (1996) 13715–13719.
- [40] J.B. Hannon, K. Pohl, P.J. Rous, E.W. Plummer, Structure of the Be(11 $\bar{2}$ 0) surface, *Surf. Sci.* 364 (1996) L617–L624.
- [41] M. Lazzeri, S. de Gironcoli, Ab-initio dynamical properties of the Be(0001) surface, *Surf. Sci.* 402 (1998) 715–718.
- [42] M. Lazzeri, S. de Gironcoli, Ab initio study of Be (10 $\bar{1}$ 0) surface dynamical properties, *Surf. Sci.* 454 (2000) 442–446.
- [43] E. Wachowicz, A. Kiejna, Bulk and surface properties of hexagonal-close-packed Be and Mg, *J. Phys. Condens. Mat.* 13 (2001) 10767–10776.
- [44] M. Lazzeri, S. de Gironcoli, First-principles study of the thermal expansion of Be(10 $\bar{1}$ 0), *Phys. Rev. B* 65 (2002) 245402.
- [45] S.J. Tang, H.T. Jeng, C.S. Hsue, Ismail, P.T. Sprunger, E.W. Plummer, Surface state influence on the surface lattice structure in Be(10 $\bar{1}$ 0), *Phys. Rev. B* 77 (2008) 045405.
- [46] G. Kresse, J. Hafner, Ab initio molecular-dynamics for liquid-metals, *Phys. Rev. B* 47 (1993) 558–561.
- [47] G. Kresse, J. Furthmüller, Efficient iterative schemes for ab initio total-energy calculations using a plane-wave basis set, *Phys. Rev. B* 54 (1996) 11169–11186.
- [48] J.P. Perdew, Y. Wang, Accurate and simple analytic representation of the electron-gas correlation-energy, *Phys. Rev. B* 45 (1992) 13244–13249.
- [49] P.E. Blochl, Projector augmented-wave method, *Phys. Rev. B* 50 (1994) 17953–17979.
- [50] G. Kresse, D. Joubert, From ultrasoft pseudopotentials to the projector augmented-wave method, *Phys. Rev. B* 59 (1999) 1758–1775.
- [51] Jmol: an open-source Java viewer for chemical structures in 3D. <http://www.jmol.org/>.
- [52] I. Langmuir, The dissociation of hydrogen into atoms. III. The mechanism of the reaction, *J. Am. Chem. Soc.* 38 (1916) 1145–1156.
- [53] A. Gross, A. Dianat, Hydrogen dissociation dynamics on precovered Pd surfaces: Langmuir is still right, *Phys. Rev. Lett.* 98 (2007) 206107.
- [54] Ch. Stihl, P.V. Vladimirov, Multiscale modelling of hydrogen behaviour on beryllium (0001) surface, *Nucl. Mat. Energy* 9 (2016) 547–553.
- [55] G. Wulff, Zur Frage der Geschwindigkeit des Wachstums und der Auflösung der Krystallflächen, *Z. Kryst. Mineral.* 34 (1901) 449–530.
- [56] C. Herring, Some theorems on the free energies of crystal surfaces, *Phys. Rev.* 82 (1951) 87–93.
- [57] R. Yu, P.K. Lam, 1st-principles total-energy study of hydrogen adsorption on Be(0001), *Phys. Rev. B* 39 (1989) 5035–5040.
- [58] P.J. Feibelman, Structure of H-covered Be(0001), *Phys. Rev. B* 48 (1993) 11270–11276.
- [59] X.F. Wang, L. Andrews, One-dimensional BeH<sub>2</sub> polymers: infrared spectra and theoretical calculations, *Inorg. Chem.* 44 (2005) 610–614.
- [60] E.N. Koukaras, A.P. Sgouros, M.M. Sigalas, Fully hydrogenated beryllium nanoclusters, *J. Am. Chem. Soc.* 138 (2016) 3218–3227.
- [61] Ismail, P. Hofmann, A.P. Baddorf, E.W. Plummer, Thermal expansion at a metal surface: a study of Mg(0001) and Be(10 $\bar{1}$ 0), *Phys. Rev. B* 66 (2002) 245414.
- [62] Y. Udagawa, M. Yamaguchi, H. Abe, N. Sekimura, T. Fuketa, Ab initio study on plane defects in zirconium-hydrogen solid solution and zirconium hydride, *Acta Mater.* 58 (2010) 3927–3938.
- [63] P.J. Feibelman, 1st-principles calculation of the geometric and electronic-structure of the Be(0001) surface, *Phys. Rev. B* 46 (1992) 2532–2539.
- [64] H.L. Davis, J.B. Hannon, K.B. Ray, E.W. Plummer, Anomalous interplanar expansion at the (0001) surface of Be, *Phys. Rev. Lett.* 68 (1992) 2632–2635.
- [65] P. Bavli, E. Polturak, J. Adler, Molecular dynamics study of melting of the hcp metal Mg, *Phys. Rev. B* 84 (2011) 235442.
- [66] W.A. Miller, G.J. Carpenite, G.A. Chadwick, Anisotropy of interfacial free energy of some hexagonal close-packed metals, *Philos. Mag.* 19 (1969) 305–319.
- [67] M. Touzani, M. Wortis, Simple-model for the equilibrium shape of He-4 crystals, *Phys. Rev. B* 36 (1987) 3598–3602.
- [68] A. Hashibon, J. Adler, G. Baum, S.G. Lipson, Roughening transitions and surface tension in an hcp lattice with higher neighbor interactions, *Phys. Rev. B* 58 (1998) 4120–4129.
- [69] R. Tran, Z. Xu, B. Radhakrishnan, D. Winston, W. Sun, K.A. Persson, S.P. Ong, Surface energies of elemental crystals, *Sci. Data* 3 (2016) 160080.
- [70] <http://crystalium.materialsvirtuallab.org/>.
- [71] U. Fischer, Y. Chen, D. Leichte, A. Moeslang, S. Simakov, P. Vladimirov, Nuclear irradiation parameters of beryllium under fusion, fission and IFMIF irradiation conditions, in: H. Kawamura, S. Tanaka, E. Ishitsuka (Eds.), *Proceedings of the Sixth IEA International Workshop on Beryllium Technology for Fusion (BeWS-6)*, Japan Atomic Energy Research Institute, Miyazaki city, Japan, 2004, pp. 146–156.
- [72] V.P. Chakin, A.O. Posevin, I.B. Kupriyanov, Swelling, mechanical properties and microstructure of beryllium irradiated at 200 degrees C up to extremely high neutron doses, *J. Nucl. Mater* 367 (2007) 1377–1381.
- [73] V. Chakin, R. Rolli, A. Moeslang, P. Vladimirov, P. Kurinskiy, S. van Til, A.J. Magielsen, M. Zmitko, Characterization of constrained beryllium pebble beds after neutron irradiation at HFR at high temperatures up to helium production of 3000 appm, *Fusion Eng. Des.* 88 (2013) 2309–2313.
- [74] I.B. Kupriyanov, R.R. Melder, V.A. Gorokhov, The effect of neutron irradiation on beryllium performance, *Fusion Eng. Des.* 51–52 (2000) 135–143.
- [75] V. Chakin, R. Rolli, A. Moeslang, P. Kurinskiy, P. Vladimirov, C. Ferrero, R. Pieritz, W. Van Renterghem, Study of helium bubble evolution in highly neutron-irradiated beryllium by using x-ray micro-tomography and metallography methods, *Phys. Scr.* T145 (2011) 014012.
- [76] M. Klimenkov, V. Chakin, A. Moeslang, R. Rolli, TEM study of beryllium pebbles after neutron irradiation up to 3000 appm helium production, *J. Nucl. Mater* 443 (2013) 409–416.
- [77] S.P. Vagin, P.V. Chakrov, B.D. Utkelbayev, L.A. Jacobson, R.D. Field, H. Kung, Microstructural study of hydrogen-implanted beryllium, *J. Nucl. Mater* 258 (1998) 719–723.
- [78] W.Z. Xu, Y.F. Zhang, G.M. Cheng, W.W. Jian, P.C. Millett, C.C. Koch, S.N. Mathaudhu, Y.T. Zhu, In-situ atomic-scale observation of irradiation-induced void formation, *Nat. Commun.* 4 (2013) 2288.